Journal of Physics: Conference Series **1561** (2020) 012002 doi:10.1088/1742-6596/1561/1/012002

Full Monte Carlo internal dosimetry in nuclear medicine by means of GAMOS

Ernesto Amato[1,2], Lucrezia Auditore[1,2,*], Antonio Italiano[2,3], Daniele Pistone[2,3], Pedro Arce[4], Alfredo Campennì[1,5], Sergio Baldari[1,5]

[1] Department of Biomedical and Dental Sciences and Morphofunctional Imaging, University of Messina, Italy
[2] Istituto Nazionale di Fisica Nucleare, Sezione di Catania, Italy
[3] MIFT Department, University of Messina, Italy
[4] Medical Applications Unit, Centro de Investigaciones Energéticas, MedioAmbientales y Tecnológicas (CIEMAT), Madrid, Spain
[5] Nuclear Medicine Unit, University Hospital "G. Martino", Messina, Italy

Corresponding author: lauditore@unime.it

Abstract. Three-dimensional internal dosimetry is increasingly used in diagnostic and therapeutic nuclear medicine. Even if simplified calculation approaches are currently available, the full Monte Carlo simulation of the radiation spectra emitted by nuclides and its interaction in living matter remains the gold standard in terms of accuracy of results. We developed a procedure exploiting the GAMOS (GEANT4-based Architecture for Medicine-Oriented Simulations) interface to GEANT4 (Geometry and Tracking 4) Monte Carlo, together with *ad-hoc* implemented ancillary codes for managing I/O. SPECT and PET images were employed to model the 3D distribution of radionuclide emissions in a voxelized volume whose density and composition was obtained from CT scan. All pre-treatments of SPECT, PET and CT images, including registration, segmentation of Volumes Of Interest (VOIs) and calculation of Time-Integrated Activity (TIA) maps for multiple time-points imaging, were carried out through either the commercial Philips Imalytics or the free 3D-Slicer software. We applied our procedure to SPECT-CT pre-therapeutic imaging with ^{99m}Tc-MAA of Trans-Arterial Radio-Embolization of hepatocellular carcinoma and to ^{18}F-Choline PET-CT scans. Three-dimensional absorbed dose maps, dose profiles and Dose-Volume Histograms (DVHs) were produced and compared with results coming from Medical Internal Radiation Dose (MIRD) approach at organ level. Discrepancies were mainly found where photon contribution to absorbed dose is dominant as well as in presence of relevant tissue inhomogeneities.

Keywords:
Internal dosimetry, Monte Carlo, GEANT4, GAMOS.

1. Introduction

In the last decades nuclear medicine treatments were increasingly employed for cancer or chronic disease diagnosis and treatment. Administration of radiopharmaceuticals to humans exposes them to risks that need to be carefully evaluated in order to guarantee both the patient's safety and, at the same time, the efficacy of therapies or diagnostic procedures. For this reason, internal dosimetry plays a more and more important role for the optimization of diagnosis and therapy in nuclear medicine [1-4].
Nevertheless, the high quality of imaging data (both morphological and functional) obtainable with the new technologies employed in diagnostic field allows to carry out accurate dosimetric estimates and to state the correspondence between internal dosimetry indicators, biological effects and therapy outcomes [5,6].
Several analytical approaches were developed in order to estimate the 3D distribution of radiation absorbed doses in organs and tissues where the radiopharmaceutical uptake is not uniform; approaches based on voxel S factors or absorbed dose point-kernels are available [7-10], but all of them suffer of limitations. The most important limitation is the uniform density assignment (generally equal to one) to materials not allowing to consider the differences between human tissues, such as lungs, adipose tissue, parenchyma, organs and bone [11,12], although some efforts have been done in order to consider heterogeneous density distribution [13]. Another limitation regards the available computational resources: the convolution methods cannot extend to an infinite range from the calculation point, but they are generally truncated to short distances from the point of interest thus neglecting the contribution of gamma-rays.

The solution to these limitations is represented by Monte Carlo (MC) approaches, enabling full radiation transport in complex geometries. Many research groups set up MC procedures using different codes (such as GEANT4, MCNPX, EGS, Fluka) allowing to implement the real patient geometry reproducing tissue inhomogeneities and the real distribution of the radiopharmaceutical within the patient's body [14-22]. The patients' information is retrieved from Computed Tomography (CT), Single Photon Emission Computed Tomography (SPECT) or Positron Emission Tomography (PET).
In this paper we discuss the performances of a computational procedure that we developed exploiting the GAMOS (GEANT4-based Architecture for Medicine-Oriented Simulations) interface [23] to GEANT4 (Geometry and Tracking 4) Monte Carlo [24], together with *ad-hoc* implemented ancillary codes for managing I/O, in performing internal dosimetry studies both for nuclear medicine diagnostic procedures and for therapy employing radiopharmaceuticals.
Among clinical PET tracers, ^{18}F-Choline is generally used for diagnosing prostate cancer [25]. The physiological uptake of ^{18}F-Choline is mainly observed in liver, pancreas, spleen, salivary and lachrymal glands and urinary tract (due to renal excretion), and it is necessary to evaluate the absorbed dose to these organs in order to estimate the risk to which the patient is exposed during the diagnostic procedure. In this paper we carried out MC simulations in order to evaluate the absorbed dose rate in liver and we compared MC results with the dose estimations made using the Medical Internal Radiation Dosimetry (MIRD) approach [26].

Trans-Arterial Radio-Embolization (TARE) of HepatoCellular Carcinoma (HCC) with ^{90}Y glass microsphere is a therapy used to treat patients with primary and secondary hepatic tumors [27,28]. In order to find a good compromise between therapy efficacy and patient safety, accurate absorbed dose estimations are needed for planning the treatment. We performed MC simulations for absorbed dose assessment in selected clinical cases and we compared the results with the dose estimations performed.

2. Materials and Methods

GAMOS allows to define a voxelized phantom reproducing the realistic patient's morphology by properly managing CT images. In particular, a bi-linear correspondence between Hounsfield Units

(HU) and density was defined in order to assign to each voxel of the phantom a density value thus reproducing the tissue inhomogeneities. Then, five intervals of density were defined in order to associate them the different chemical composition of materials (air: 0.0-0.1 gcm^{-3}; lung: 0.1-0.85 gcm^{-3}; adipose tissue: 0.85-0.94 gcm^{-3}; soft tissue: 0.94-1.2 gcm^{-3}; bone: >1.2 gcm^{-3}). The number of materials was properly chosen to take into account the main density inhomogeneities of the human body in the districts of interest.

The voxelized phantom includes the definition of Volumes Of Interest (VOIs) segmented on the SPECT-CT or PET-CT images by an experienced operator (the same for all the segmentations considered in this study) on the Philips Imalytics Research Workstation [29].

The realistic radiopharmaceutical distribution was retrieved from the functional images (SPECT or PET), properly transformed in a text file used by GAMOS as the source probability distribution by means of the generator class named `GmGenerDistPositionInVoxelsFromFile`.

The complete radioactive decay of the isotope was simulated using the *RadioactiveDecay* module of GEANT4 [30], whose models are based on Evaluated Nuclear Structure Data File (ENSDF) [31,32].

An extended electromagnetic physics list, the *GmEMExtendedPhysics* package [30], was used: it uses the Livermore low energy electromagnetic physics model and enables the atomic de-excitation.

A range cut of 50 μm was set allowing us to accurately sample spatial distribution of energy deposition. 10^8 events per simulation were generated in order to obtained results with associated statistical uncertainties (2σ) below 5%. No variance reduction method was used.

As MC simulations results, we estimated the mean absorbed doses in VOIs and compared with the estimates obtained with the MIRD approach. Moreover, we obtained the 3D absorbed dose maps and the Dose Volume Histograms (DVH) in the considered VOIs.

2.1. ^{18}F-Choline PET dosimetry

Choline is a precursor for the biosynthesis of phospholipids, which are the major components of the cellular membrane. Radiolabeled choline, such as ^{18}F-Choline, allows to detect tumors, in particular prostate cancer, because of the enhanced choline uptake due to the increased demand for cellular membrane synthesis.

The State-of-the-art dosimetry of PET diagnostic tracers can help in optimizing the procedure in view of the balance between radiation risk and diagnostic information. A particular attention has to be paid to high-uptake organs and in particular to liver which synthesizes the molecule. In this paper we report, as an example, the internal dosimetry for a male patient administered with 296 MBq of ^{18}F-Choline.

PET-CT acquisitions were performed with a Philips Gemini 16 TF scanner; 510 CT slices (each of 256x256 pixels), were processed to build the voxelized phantom in MC simulations; each phantom voxel had dimensions equal to 2.34x2.34x2.0 mm^3; 55 PET slices (each of 144x144 pixels) calibrated in Bq/mL, were used to define the source probability distribution map in order to generate events reproducing the realistic bio-distribution of ^{18}F-Choline at the scan time.

The VOI representing the liver was segmented on the CT images and MC simulations were carried out to evaluate the average absorbed dose rate and a Dose-Volume Histogram in the selected VOI, together with the 3D absorbed dose rate map extended to the entire patient's body.

The mean absorbed dose rate in liver was then calculated by OLINDA/EXM software [26] and compared with the values obtained by the MC simulations. OLINDA/EXM assumes a uniform radiopharmaceutical distribution in the target organ and considers an anthropomorphic phantom allowing to personalize organs' masses.

2.2. TARE dosimetry

In TARE of HCC, a pre-therapeutic dosimetric study is required for treatment planning. First, the evaluation of the absorbed dose to lesions gives information on the expected efficacy of the treatment and on the activity to be administered; second, the evaluation of the absorbed dose to critical organs (healthy liver and lungs) limits the activity to be administered to the patient.

The dosimetric study is based on a contrast-enhanced CT for the lesion localization and (planar and tomographic) scintigraphic imaging of ^{99m}Tc-labeled Macro-Aggregates of Albumin (MAA) selectively intra-arterial administered in liver, in order to make previsions on the distribution in liver of the ^{90}Y-labelled glass microspheres and to evaluate pulmonary shunt.

In the case reported, internal dosimetry was carried out for a male patient, to whom 185 MBq of ^{99m}TC-MAA were administered for the preliminary diagnostic procedure and 4.19 GBq of ^{90}Y-labelled glass microspheres were administered for the treatment; 141 CT slices (each of 512x512 pixels) were processed to build the voxelized phantom used in the MC simulations. Each voxel had dimensions of 0.78x0.78x2.0 mm^3. Planar and SPECT images were acquired with a Philips BrightView Dual Head gamma camera equipped with low-energy, general-purpose collimators. 42 SPECT slices (each of 128x128 pixels) were reconstructed through iterative OSEM algorithm in cubic voxels, 4.664 mm in side. The SPECT images were used in the MC simulations as the ^{90}Y source probability distribution.

Five VOIs were defined: Liver and Lesion segmented on contrast-enhanced CT (arteriographic phase); Liver Perfused segmented on SPECT; Healthy Liver obtained by a logical subtraction of Lesion from Liver; Healthy Liver Perfused obtained by a logical subtraction of Lesion from Liver Perfused.

Since ^{90}Y-labelled glass microspheres induce embolization, stopping in the capillary where they are delivered, no biological clearance of ^{90}Y has to be considered, so that its decay can be treated as a pure physical decay process. In such conditions, the Time-Integrated Activity (TIA) in each voxel of the simulated phantom can be estimated as [33]:

$$\tilde{A}^{ijk} = A_0^{ijk}\tau \tag{1}$$

where A_0^{ijk} is the fraction of the administered activity reaching the (i,j,k) voxel and τ is the physical decay time of the nuclide. The TIA was then used to estimate the total number of disintegration needed to convert the MC results from Gy/event to Gy.

MC evaluations were then compared with the dose values obtained by an analytical approach. According to the MIRD approach, the absorbed dose (in Gy) to the soft tissue target can be calculated as [34, 35]:

$$D = 49.67 \cdot \frac{A_0}{m} \tag{2}$$

where A_0 is the administered activity, in GBq, and m is the target mass, in kg. Eq. (2) does not take into account radiopharmaceutical uptake inhomogeneities and assumes a complete, local energy deposition within the target.

3. Results and discussion

3.1. ^{18}F-Choline PET dosimetry

In subfigures 1(a-c) axial, sagittal and coronal projections of the fusion of CT and PET images are shown, while subfigures 1(d-f) report the same projections of the fusion of CT images and absorbed dose rate map. The dose rate map correctly reflects both the radiopharmaceutical distribution and the density inhomogeneities of the human body.

The green line in subfigure 1a) represents the segmented liver. The average absorbed dose rate in liver VOI (1074.35 cm^3) was estimated as 84.3 μGy/min. Dose Rate Volume Histogram (DRVH) for liver is reported in Figure 2, showing that for about half of liver volume the absorbed dose rate is less than 85 μGy/min.

Absorbed dose rate in Liver was also estimated by means of OLINDA/EXM software [26] and resulted equal to 75 μGy/min; this calculation was based on a liver mass of 1117 g and a total activity in liver at the PET scan time of 23.1 MBq. OLINDA/EXM underestimates the dose rate to liver of about 11% with respect to MC simulations.

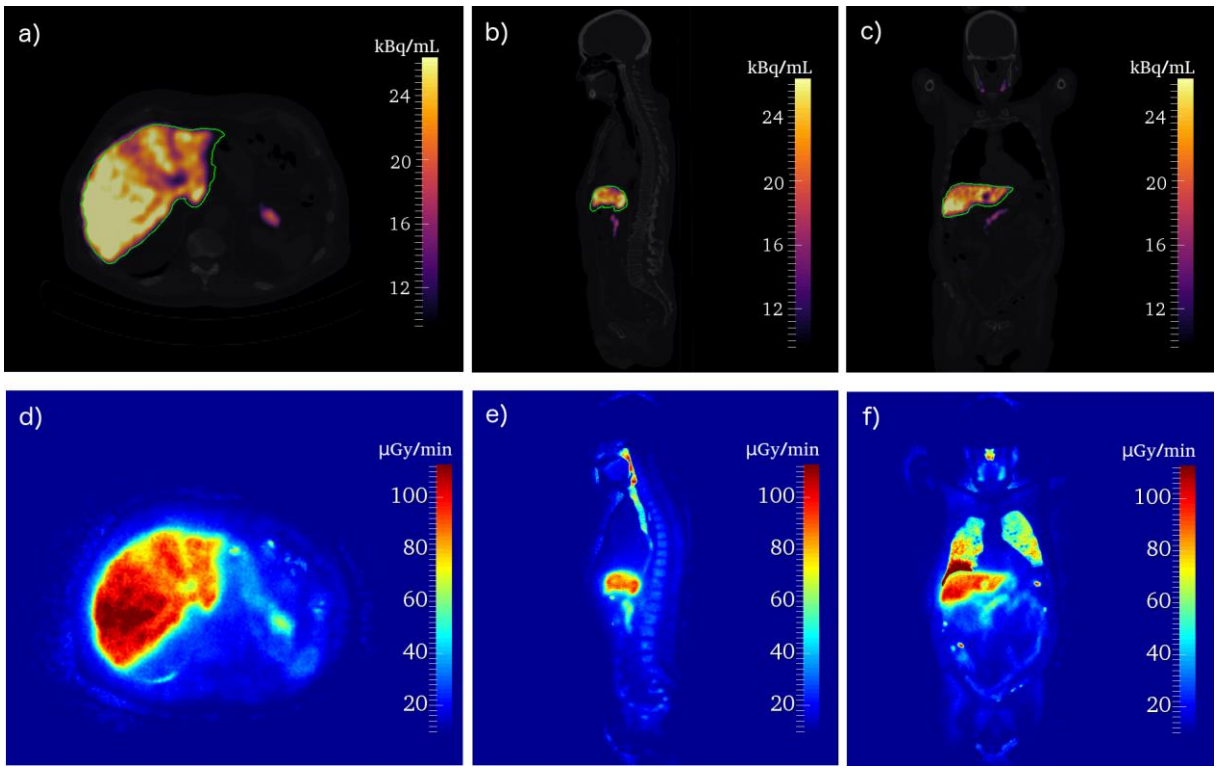

Figure 1. (a) axial, (b) sagittal and (c) coronal projections of the fusion of a CT slice and ^{18}F-Choline PET image. (d) axial, (e) sagittal and (f) coronal projections of the absorbed dose rate map as resulting from MC simulations.

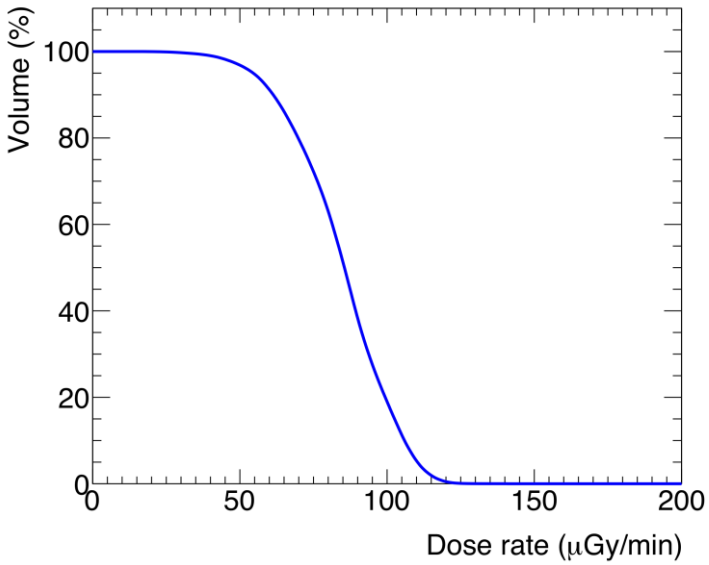

Figure 2. DRVH computed for the Liver VOI by means of the analysis of the 3D dose rate map obtained with MC simulations.

3.2. TARE dosimetry

In subfigures 3(a-c) axial, sagittal and coronal projections of the fusion of CT and SPECT images are shown. To make images easy to read only two VOIs are represented: Liver Perfused (green line) and Lesion (light blue line). The three projections of the fusion of CT images and absorbed dose rate map are reported in subfigures 3(d-f).

In Figure 4 we report the Dose Rate Volume Histogram for the segmented VOIs as computed by analyzing 3D dose rate maps resulting from MC simulations.

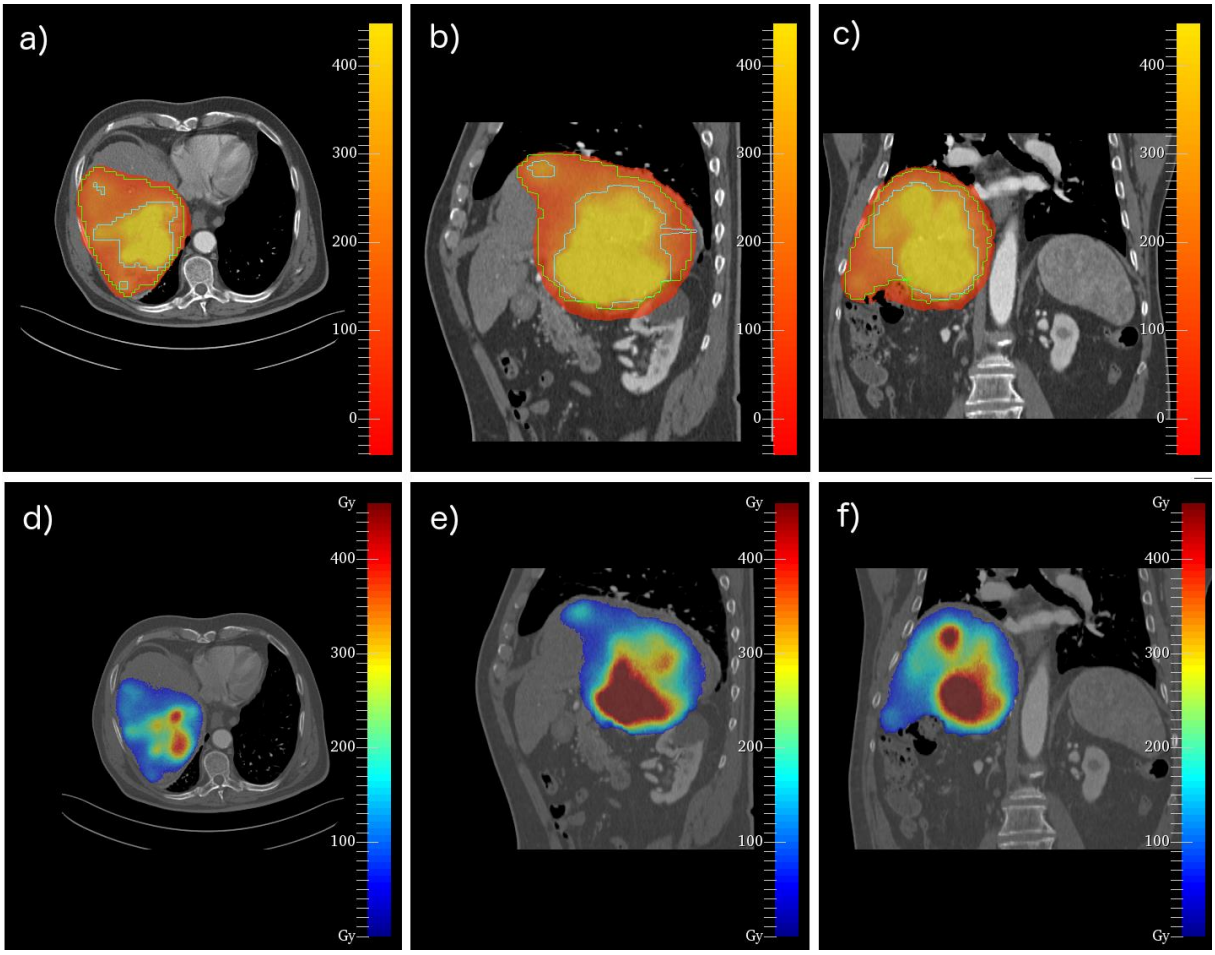

Figure 3. (a) axial, (b) sagittal and (c) coronal projections of the fusion of a CT slice and the corresponding SPECT image. Green and light blue lines indicate the contours of Liver Perfused and Lesion VOIs, respectively; (d) axial, (e) sagittal and (f) coronal projections of the fusion of the same CT slice as before and the corresponding absorbed dose rate map as resulting from MC simulations.

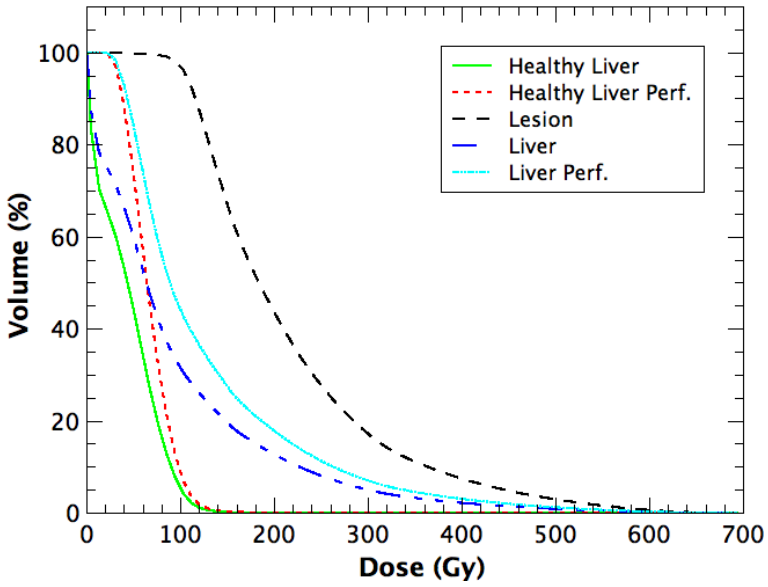

Figure 4. Dose Volume Histograms computed by means of MC simulations for the five VOIs defined in TARE case.

Estimations of the absorbed dose to the five VOIs, computed by MC simulation (D_{MC}) and MIRD approach (D_{MIRD}), are reported in Table 1; in order to compare the two approaches, the relative percent differences between the estimations, ε(%), calculated as:

$$\varepsilon\,(\%) = 100 \cdot \frac{D_{MIRD} - D_{MC}}{D_{MC}}$$

are also displayed.
Liver Perfused receives 126.2 Gy, in agreement with the dose recommended for the treated liver lobe (120-140 Gy) to guarantee the patient's safety; lesion receives a dose of 213.3 Gy advisable for the success of TARE treatment.
MIRD approach-based evaluations agree with MC estimates for all but one of VOIs, Healthy Liver, probably due to the gamma interactions properly modeled only by MC simulations.

Table 1. Values of absorbed dose to the five VOIs estimated by the two calculation methods: MC simulations (D_{MC}) and MIRD approach (D_{MIRD}). Relative percent differences, ε (%), of MIRD *vs*. MC estimations are also reported.

	D_{MC} (Gy)	D_{MIRD} (Gy)	ε (%)
Healthy Liver	10.5	12.2	16.83
Healthy Liver Perfused	65.4	65.8	0.55
Lesion	213.3	216.4	1.45
Liver	94.2	92.4	-1.96
Liver Perfused	126.2	131.6	4.25

4. Conclusions

MC simulations are a powerful tool to carry out internal dosimetry with the aim to optimize diagnostic and therapeutic procedures. Despite many analytical calculation approaches based on voxel S factors or local energy deposition methods, MC simulations allow to accurately reproduce the patient's morphology (from CT data) and the actual radiopharmaceutical distribution in the patient's body (from PET or SPECT data), also properly modeling gamma interaction.
The two cases reported in this paper are two examples indicating how MC simulations can be successfully applied to both diagnostic and therapeutic internal dosimetry studies, for the purposes of optimizing the risk connected with the use of radiopharmaceuticals in diagnostic procedures, or for the pre-treatment evaluation of the effectiveness of radionuclide therapies.
Moreover, the comparison between MC dosimetry and organ-level dosimetry shows that, despite MC simulations are carried out by complex and time-consuming procedures, their use appears more appropriate where tissue density inhomogeneities or uneven radiopharmaceutical distributions are relevant.

References

[1] Stokke C, Gabiña PM, Solný P, Cicone F, Sandström M, Gleisner KS et al. 2017 *EJNMMI Phys* **4** 27
[2] Minutoli F, Amato E, Sindoni A, Cardile D, Conti A, Herberg A, Baldari S. 2014 *Cancer Biother Radiopharm* **29** 193
[3] Amato E, Campennì A, Leotta S, Ruggeri RM, Baldari S. 2016 *Phys Medica* **32** 847
[4] Amato E, Cicone F, Auditore L, Baldari S, Prior JO and Gnesin S 2018 *Phys Medica* **49** 52
[5] Li T, Ao ECI, Lambert B, Brans B, Vandenberghe S and Mok GSP 2017 *Technical Review. Theranostics* **7** 4551
[6] Strigari L, Konijnenberg M, Chiesa C, Bardies M, Du Y, Gleisner KS et al. 2014 *Eur J Nucl Med Mol Imaging* **41** 1976
[7] Amato E, Minutoli F, Pacilio M, Campennì A and Baldari S 2012 *Med Phys* **39** 6808
[8] Giap HB, Macey DJ, Bayouth JE and Boyer AL 1995 *Phys Med Biol* **40** 365
[9] Dieudonné A, Garin E, Laffont S, Rolland Y, Lebtahi R, Leguludec D and Gardin I 2011 *J Nucl Med* **52** 1930
[10] Kafrouni M, Allimant C, Fourcade M, Vauclin S, Delicque J, Ilonca A-D, Guiu B, Manna F, Molinari N, Mariano-Goulart D and Bouallgue FB 2018 *J Nucl Med* **59** 1289
[11] Amato E, Italiano A and Baldari S 2013 *Nucl Instruments Methods Phys Res Sect A Accel Spectrometers, Detect Assoc Equip* **729** 870
[12] Khazaee Moghadam M, Kamali Asl A, Geramifar P and Zaidi H 2016 *Cancer Biother Radiopharm* **31** 367
[13] Sanchez-Garcia M, Gardin I, Lebtahi R and Dieudonné A 2015 *Phys. Med Biol* **60** 7861
[14] Furhang EE, Chui CS, Kolbert KS, Larson SM and Sgouros G 1997 *Med Phys* **24** 1163
[15] Yoriyaz H, Stabin MG and dos Santos A 2001 *J Nucl Med* **42**(4) 662
[16] Ljungberg M, Sjögreen K, Liu X, Frey E, Dewaraja Y and Strand SE 2002 *J Nucl Med* **43**(8) 1101
[17] Marcatili S, Pettinato C, Daniels S, Lewis G, Edwards P, Fanti S et al. 2013 *Phys Med Biol* **58** 2491
[18] Grimes J, Uribe C and Celler A 2013 *Med Phys* **40** 072501

[19] Kost SD, Dewaraja YK, Abramson RG and Stabin MG 2015 *Cancer Biother Radiopharm* **30** 16
[20] Besemer AE, Yang YM, Grudzinski JJ, Hall LT and Bednarz BP 2018 *Cancer Biother Radiopharm* **33** 155
[21] Petitguillaume A, Bernardini M, Hadid L, De Labriolle-Vaylet C, Franck D and Desbrée A 2014 *J Nucl Med* **55** 405
[22] Hashikin NAA, Yeong CH, Guatelli S, Abdullah BJJ, Ng KH, Malaroda A, Rosenfeld A and Perkins AC 2017 *Phys Med Biol* **62** 7342
[23] Arce P, Rato P, Cañadas M and Lagares JI 2008 *2008 IEEE Nucl. Sci. Symp. Conf. Rec.* 3162
[24] Agostinelli S et al. 2003 *Nucl Instrum Methods A* **506** 250
[25] Mapelli P, Incerti E, Ceci F, Castellucci P, Fanti S, Picchio M. 2016 *J Nucl Med* **57** 43S
[26] Stabin M G, Sparks RB, Crowe E 2005 *J Nucl Med* **46** 1023
[27] Auditore L, Amato E, Italiano A, Arce P, Campennì A and Baldari S 2019 *Phys Med* **64** 245
[28] Amato E, Lizio D. 2009 *J Radiol Prot* **29** 239
[29] Paulus T, Fischer A, van Loon P, Schweizer B, Gegenmantel E and Bippus R 2010 *Medicamundi* **54**(2) 78
[30] Geant4 Reference Physics Manual, version geant4 10.3, n.d. http://geant4.cern.ch.
[31] ENSDF, Evaluated Nuclear Structure Data File, Maint. by Natl. Nucl. Data Cent. Brookhaven Natl. Lab. (n.d.). http://www.nndc.bnl.gov/ensdf/.
[32] Tuli J 1987 Evaluated nuclear structure data file, BNL-NCS-51655-Rev87.
[33] Bolch WE, Eckerman KF, Sgouros G, Thomas SR, Brill AB, Fisher DR et al. 2009 *J Nucl Med* **50** 477
[34] Ho S, Lau WY, Lung TWT, Chan M, Ngar YK, Johnson PJ and Li AKC 1996 *Eur J Nucl Med* **23**(8) 947
[35] Chiesa C, Mira M, Maccauro M, Spreafico C, Romito R, Morosi C et al. 2015 *Eur J Nucl Med Mol Imaging* **42** 1718